DOI 10.1515/aot-2014-0006 — Adv. Opt. Techn. 2014; 3(2): 141–150

Tutorial

Quankui Yang, Frank Fuchs and Joachim Wagner*

Quantum cascade lasers (QCL) for active hyperspectral imaging

Abstract: There is an increasing demand for wavelength agile laser sources covering the mid-infrared (MIR, 3.5–12 μm) wavelength range, among others in active imaging. The MIR range comprises a particularly interesting part of the electromagnetic spectrum for active hyperspectral imaging applications, due to the fact that the characteristic 'fingerprint' absorption spectra of many chemical compounds lie in that range. Conventional semiconductor diode laser technology runs out of steam at such long wavelengths. For many applications, MIR coherent light sources based on solid state lasers in combination with optical parametric oscillators are too complex and thus bulky and expensive. In contrast, quantum cascade lasers (QCLs) constitute a class of very compact and robust semiconductor-based lasers, which are able to cover the mentioned wavelength range using the same semiconductor material system. In this tutorial, a brief review will be given on the state-of-the-art of QCL technology. Special emphasis will be addressed on QCL variants with well-defined spectral properties and spectral tunability. As an example for the use of wavelength agile QCL for active hyperspectral imaging, stand-off detection of explosives based on imaging backscattering laser spectroscopy will be discussed.

Keywords: active hyperspectral imaging; quantum cascade lasers.

***Corresponding author: Joachim Wagner,** Fraunhofer-Institut für Angewandte Festkörperphysik, Tullastrasse 72, 79108 Freiburg, Germany, e-mail: joachim.wagner@iaf.fraunhofer.de
Quankui Yang and Frank Fuchs: Fraunhofer-Institut für Angewandte Festkörperphysik, Tullastrasse 72, 79108 Freiburg, Germany

1 Introduction

Quantum cascade lasers (QCLs) are unipolar semiconductor lasers whose operation is entirely based on quantum mechanics [1]. In Figure 1, the conduction band profile as well as the energy subbands and associated electron probability densities (wavefunctions squared) are shown for a typical GaInAs/AlInAs-on-InP QCL structure under applied bias voltage corresponding to an internal electric field of F=70 kV/cm. The lasing transition occurs between electron subbands formed in the conduction band of typically a few nm-thick layers, so-called quantum wells (QWs), of a semiconductor with smaller bandgap energy, e.g., GaInAs. The QWs are embedded between barrier layers made from a semiconductor with larger bandgap energy, e.g., AlInAs. The lasing wavelength of a QCL is given by the energy separation between two subbands, which constitute the upper and lower laser levels, respectively. The optical transitions are indicated in Figure 1 as red arrows. This energy separation, which determines the emission wavelength, is primarily determined by the width of the QW layers in the active region. Electron transport, required to establish a vertical current flow through the stack of alternating QW and thin barrier layers for electrical pumping, is brought about by quantum mechanical tunneling of conduction band electrons through the barriers separating the QWs forming the active region, as well as through the miniband connecting neighboring active regions (shaded areas in Figure 1). Prevention of electrons to escape from the upper laser state to the continuum is obtained by using the minigaps, in which the electron density of states is minimized, as indicated in Figure 1. To enhance the optical gain, typically several 10 active region sections are stacked. The active region sections are connected by so-called injector regions. In the injector region, the electrons exiting from the laser ground state of one active region stage are reconfigured for subsequent re-injection into the upper laser level of the next active region further downstream. This way through a cascade of active regions, electrons get multiple chances to emit a photon while traversing the QCL structure.

Lacking the constraint that the emitted photon energy must equal the active region bandgap energy, which applies to classical semiconductor interband diode lasers, QCLs extend the semiconductor laser spectral gamut into

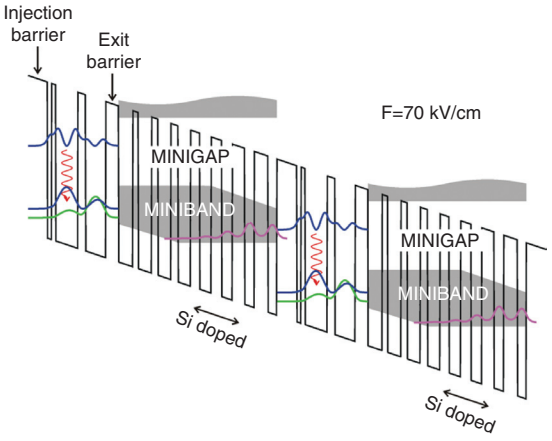

Figure 1 Conduction band profile as well as energy subbands and associated electron probability densities (wavefunctions squared) of a typical GaInAs/AlInAs-on-InP QCL structure under applied bias voltage corresponding to an internal electric field of 70 kV/cm.

the infrared and sub-millimeter (THz) spectral range. The spectral coverage of a QCL is determined primarily by its design features, but not by the fundamental band gap energy. Any wavelength within the aforementioned 3.5–12 µm MIR wavelength range can be generated by QCLs based on the same GaInAs/AlInAs/InP material system. For this particular materials combination, thanks to the fiber-based optical communication also based on this material system, a reliable QCL growth and processing technology has already been established [2–4].

2 State-of-the-art of high-power QCL

Regarding the fabrication and configuration of QCL chips, there are two main variants, namely, double-trench (DT-) QCL and buried-heterostructure (BH-) QCL. They differ in the way how the lateral optical waveguide is formed. The lateral optical waveguide confines the optical field in the lateral direction (ridge width direction), and the longitudinal modes oscillate within the Fabry-Perot type cavity formed by the cleaved facets of the QCL chip. Both the above-mentioned QCL variants share the same single-mode vertical (fast axis) waveguide, which is formed along the epitaxial growth direction by sandwiching the said GaInAs/AlInAs active regions between appropriately designed GaInAs separate confinement layers and InP cladding layers. The DT-QCL and BH-QCL differ, however, in the in-plane lateral (slow axis) waveguide design. For the DT-QCL case, the lateral waveguide is formed by two deeply etched trenches (see Figure 2), whereas for the BH-QCL case, the laser ridge is overgrown laterally

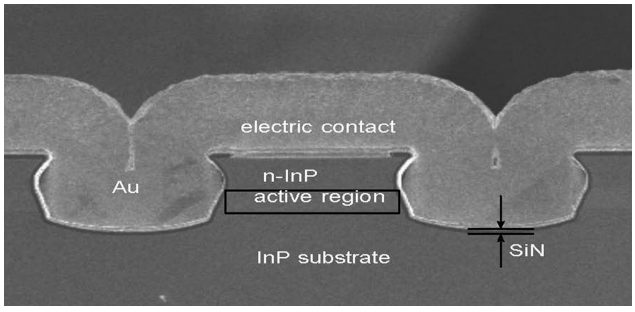

Figure 2 Cross-sectional SEM micrograph of a DT-QCL. Laser emission is perpendicular to the drawing plane. The borders of the active region have been redrawn for better contrast.

by semi-insulating InP acting as cladding material. In the latter case, an almost symmetrical waveguide (with respect to the vertical and lateral directions) is formed, and this results in an almost symmetrical near-field and far-field beam profile. With BH configuration, furthermore, a stable single-mode profile in the lateral direction can be readily achieved. Compared to BH-QCLs, DT-QCLs have the advantage of being easier to fabricate, as a second regrowth step is required for BH-QCL. However, the lateral waveguide of a DT-QCL tends to support higher-mode operation, in particular, at higher output power. Also, the lateral heat dissipation of a DT-QCL is inferior to that of a BH-QCL [1]. Figures 2 and 3 show cross-sectional scanning electron microscope (SEM) images of a standard DT-QCL and a prototypical BH-QCL, respectively.

High output power and power efficiency of MIR QCLs have been reported by, e.g., the group at Northwestern University [3]. Using strain-compensated GaInAs/AlInAs-on-InP QCL designs, this group reported a maximum output power in pulsed-mode operation (500 ns pulse length, 5% duty cycle) of 10 W at room temperature (298 K/25°C), and a corresponding maximum electrical-to-optical power

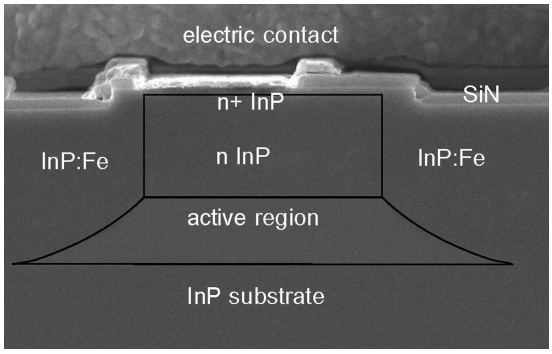

Figure 3 Cross-sectional SEM micrograph of a BH-QCL. Laser emission is perpendicular to the drawing plane. The borders of the active region as well as the cladding layer grown on top have been redrawn for better contrast.

conversion efficiency of 27%. These laboratory data were obtained for QCLs emitting at 4.9 µm, with 19-µm-wide DT ridges and a resonator length of 3 mm [5]. Using BH-QCL configuration with a ridge width of 8 µm and a resonator length of 5 mm, a maximum continuous-wave (cw) output power of 5.1 W at 25°C has been reported, with a corresponding maximum power efficiency of 21% [5]. There is also recent effort in realizing QCLs lasing at wavelengths >6 µm with output power exceeding the 1-W level [6–9]. At a lasing wavelength of 6.1 µm, a maximum cw output power of 1.2 W has been reported at a heat sink temperature of 15°C for BH-QCL, decreasing to 0.8 W at a lasing wavelength of 9 µm [6]. At an emission wavelength near 9 µm, Lyakh et al. achieved a maximum pulsed (cw) room temperature output power and power efficiency of 4.5 W (2 W) and 16% (10%), respectively, by using a BH QCL chip with a cavity length and waveguide width of 3 mm and 10 µm, respectively [8]. Most recently, at an even longer wavelength of 10.3 µm, a maximum cw output power of 1.3 W has been achieved at a heat sink temperature of 20°C, again using BH-QCL technology [9].

It has to be noted that the maximum achievable cw output power of a QCL chip depends also on the mounting technology. The chips can be mounted either epitaxial side up or epitaxial side down. The latter provides improved heat dissipation. The maximum cw output power depends furthermore on the type of heat spreader employed, such as AlN or diamond, as well as design and material of the submount used, as detailed, e.g., in Ref. [4].

A feature common to all high-power Fabry-Perot QCL is the large spectral width of the laser emission. The spectra width of a QCL can reach several percent of the central lasing wavelength at maximum output power. This large spectral width originates partly from the Stark effect, i.e., the energy separation between the upper laser level, and the lower laser level changes slightly when the voltage applied across the active region varies. Another contribution to the large spectral width is the broadening, both homogeneous and inhomogeneous, of the gain spectrum of the active region of the QCL. Figures 4 and 5 display typical high-power lasing spectra of a 4.6-µm and a 9.1-µm Fabry-Perot QCL, respectively. The QCLs were operated in short pulse mode with a duty cycle of 0.05%, showing highly multimode laser emission. Such spectrally broad Fabry-Perot QCLs are well suited as illumination source for active imaging in the MIR wavelength range, provided there are no specific requirements with respect to wavelength precision and spectral resolution. If narrow linewidth emission and spectral tunability are required to achieve sufficient spectral resolution for, e.g., imaging spectroscopy in the MIR range, more refined QCL variants are needed as will be detailed in the following sections.

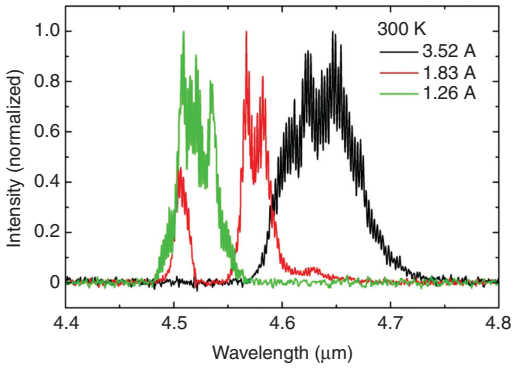

Figure 4 Current-dependent multiple-mode lasing spectra of an as-cleaved 4.6-µm emitting QCL operated in pulsed mode (100 ns pulse length, 5 kHz repetition rate) at a maximum peak power of 12 W (counted for both facets) at 3.52 A.

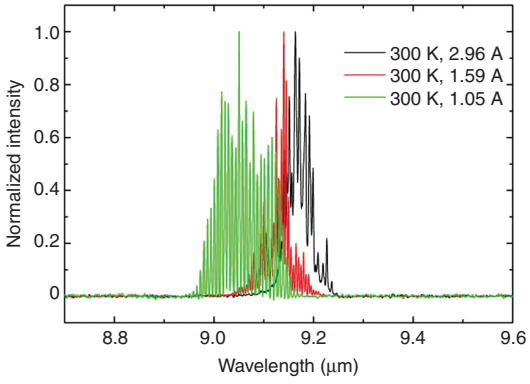

Figure 5 Current-dependent multiple-mode lasing spectrum of an as-cleaved 9.1-µm emitting QCL operated in pulsed mode (100 ns pulse length, 5 kHz repetition rate) at a maximum peak power of 1.0 W (counted for both facets) at 2.96 A.

3 Narrow linewidth QCL

A concept to generate narrow linewidth emission from a ridge-waveguide semiconductor laser is the adoption of distributed feedback (DFB) structures in the laser [10]. This concept has been already well-proven for classical semiconductor diode lasers. The DFB concept relies on an optical grating integrated in the ridge waveguide along the laser cavity direction for wavelength selection and stabilization. To minimize additional waveguide losses in a QCL, the grating is typically realized as an index grating [11, 12]. This can be formed by etching periodic groves into the upper high refractive index GaInAs separate confinement

layer of the vertical waveguide. After etching, the process is followed by the overgrowth of the top cladding layer composed of lower refractive index material (InP). Figure 6 shows a cross-sectional SEM micrograph of a GaInAs/AlInAs/InP-based DFB-QCL [13–15]. The QCL chip has been cleaved through the ridge waveguide, with the cleavage plane along the waveguide axis. The optical mode propagates horizontally through the waveguide, and this way interacts with the refractive index grating formed by the upper GaInAs (lattice matched to InP) separate confinement layer and the overgrown InP top cladding layer.

If the optical stop band generated by the periodic grating sufficiently overlaps with the gain spectrum of the QCL active region, a single mode at the stop-band edge will be feedback and enhanced. This way the emission spectrum will consist of one single-mode with its wavelength pinned to the resonance wavelength of the grating. The resonance wavelength of a DFB-QCL depends on both the grating period and the effective refractive index of the waveguide (The Bragg equation reads: $2d=\frac{m\lambda_0}{n_{\text{eff}}}$, where m is the order of grating, λ_0 is the emission wavelength in free space, d is the grating period, and n_{eff} is the effective refractive index). The effective refractive index n_{eff} is a function of the device temperature. Thus, the emission wavelength of a DFB-QCL can be tuned by heating or cooling the DFB-QCL chip-on-submount as a whole, as illustrated in Figure 7, or by just varying the injection current, which will cause a change in the QCL active region temperature [13, 14]. The temperature coefficient of the refractive index for the relevant semiconductor materials yields a typical temperature tuning rate of the grating resonance of 0.1–0.2 cm^{-1}/K. Combined with the available temperature tuning range, which is typically a few ten Kelvins for most practical purposes, the tuning range $\Delta\lambda$ achieved this way is only in the range of a few wavenumbers. This translates into a relative tuning range of only a fraction of a percent. This tuning range is sufficient for applications such as high-resolution gas spectroscopy. Figure 8 shows a compilation of the lasing wavelengths of a series of DFB-QCLs fabricated at Fraunhofer IAF with various DFB grating periods. The emission wavelengths are well matched to strong molecular vibrational absorption bands of CO, NO, and N_2O [13, 14]. DFB-QCLs are currently becoming the workhorse for laser-based high-resolution gas spectroscopy in spectroscopic sensing and production control [16], and they are now commercially available for a wide wavelength range [17].

To widen the wavelength coverage of QCLs, a straightforward approach is to fabricate DFB chips with diverse

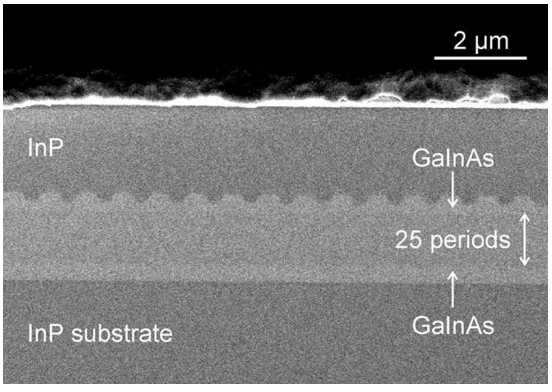

Figure 6 Cross-sectional SEM micrograph of a DFB-QCL cleaved along the resonator axis. The DFB grating was etched into the top GaInAs separate confinement layer and overgrown with InP [13, 14].

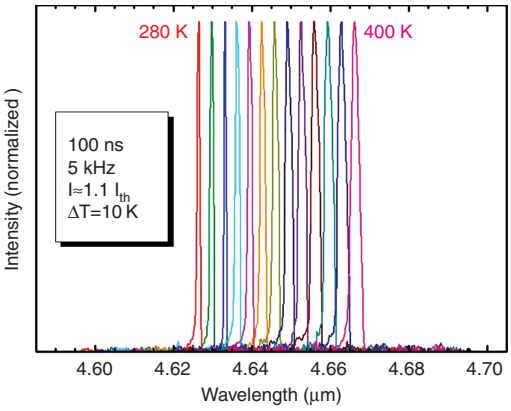

Figure 7 Temperature-dependent pulsed (100 ns pulse width, 5 kHz repetition rate) single-mode emission spectra of a GaInAs/AlInAs/InP DFB QC laser with a grating period of Λ=720 nm, covering the 280 K–400 K temperature range (10 K temperature intervals) [13, 14].

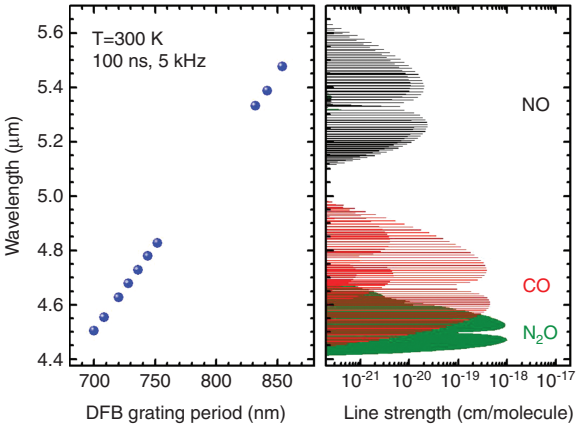

Figure 8 (A) Pulsed emission wavelength λ of single-mode DFB QCL at a heat-sink temperature of 300 K vs. DFB grating period. (B) Line strength vs. wavelength of NO, N_2O, and CO at a temperature of 296 K and atmospheric pressure calculated from the HITRAN96 database [13, 14].

grating periods on the same wafer, given that the active region of the QCL wafer has a sufficiently broad gain spectrum [18]. Another approach is to combine an array of DFB-QCLs with slightly different grating periods on a single chip [19]. This way, the coarse wavelength selection can be achieved by addressing a designated DFB-QCL on that chip, whereas continuous fine tuning can be achieved, as described above, by temperature tuning for that single DFB-QCL.

For applications such as hyperspectral imaging, high output power is deserved. To increase the output power of single-emitter DFB-QCLs and DFB-QCL arrays, ridge-waveguide DFB-QCLs have been monolithically integrated with tapered QCL amplifier sections. It has been shown that this integration significantly boosts the pulsed mode output power, from typically a few hundred mW to well above the 1-W level [20, 21]. Beam combining of multi-spectral output of such a DFB-QCL array can be achieved, either using free-space optics employing a grating-based beam combiner [22, 23], or by integrating optics on-chip using waveguide couplers [24].

Attempts have also been made to increase the tuning range of a single-emitter DFB-QCL by combining two closely coupled DFB grating sections with different grating periods. Applying different drive currents to the two grating sections in a synchronized way and exploiting the Vernier effect, the lasing wavelength of the DFB-QCL can be tuned over a spectral range wider than that achieved when using just a single period DFB grating [25]. In Ref. [26], a dual-section, single-mode quantum cascade laser was demonstrated in continuous wave at room temperature with up to 114 nm (50 cm^{-1}) of tuning near a wavelength of 4.8 μm, with a mean side-mode suppression ratio of 24 dB. By changing the grating period, 270 nm (120 cm^{-1}) of gap-free electrical tuning for a single gain medium has been realized.

Another more explorative approach to achieve wavelength tuning of QCL is to use a monolithic ridge-waveguide Mach-Zehnder type interferometer with asymmetric arms [27]. By applying different drive currents to the two arms of the interferometer, single-mode emission has been demonstrated over a tuning range of 20 cm^{-1} at a center frequency of 2080 cm^{-1}, or in other words, $\Delta\lambda/\lambda \approx 1\%$ [27].

4 Widely tunable external cavity QCL

To achieve continuous spectral tunability over an extended wavelength range, the Fabry-Perot cavity of a ridge-waveguide semiconductor laser can be coupled to an external cavity, which provides wavelength-selective optical feedback [28]. A widely used concept, frequently applied also to QCL [29, 30], is the Littrow configuration [31]. In the Littrow configuration, an optical grating acts as a wavelength-selective mirror, with the first-order diffracted light being coupled back into the semiconductor waveguide.

Figure 9 shows the schematic of an external cavity QCL (EC-QCL) in Littrow configuration. In this implementation, the output beam of the EC-QCL is coupled through the facet of the QCL chip opposite to that facing the external cavity [32]. Two large numerical aperture (NA) lenses with short working distance are employed to collimate the highly divergent output beam of the QCL waveguide. To suppress the intrinsic Fabry-Perot modes generated by the facets of the QCL cavity, the facet facing the external cavity is anti-reflection coated. The effect of anti-reflection coating of this facet is two folds: it not only increases the loss of the intrinsic Fabry-Perot modes, thus suppresses the intrinsic modes, but also enhances the coupling of light to the external cavity. The lower the residual reflectivity of the anti-reflection coating, the stronger the coupling of the QCL to the external cavity, and thus, the larger the tuning range achievable for a given width of the QCL gain spectrum. The output facet is partially reflecting, left either uncoated or with a dielectric coating applied to increase or decrease its reflectivity with respect to the Fresnel reflectivity ($R \approx 0.28$) of the uncoated facet. To enable mode-hop free tuning of the EC-QCL, the length of the external cavity has to be adjusted accordingly [33], to ensure the emission at just a single cavity mode defined by the external cavity.

The tuning range of an EC-QCL is primarily determined by the width of the gain spectrum of the QCL active region. As one of the attractive features of QCL technology, not only the emission wavelength can be engineered but also the width of the gain spectrum. The exemplary QCL active region shown in Figure 1 is based on a basic bound-to-bound design, i.e., both the upper and the lower laser levels are discrete quantized energy states, yielding a limited width of the associated gain spectrum. Actually,

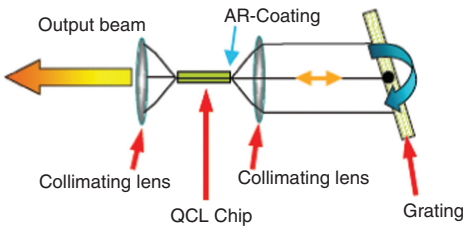

Figure 9 Schematic of an EC-QCL in Littrow configuration. The output beam is emitted from the QCL chip facet opposite to the external cavity formed by a collimating lens and the diffraction grating [32].

the lower laser level can also be engineered as a multitude of closely spaced energy states [34]. This multitude of closely spaced levels effectively forms a continuum of energy states, taking into account the finite lifetime-limited width of each level. This QCL design variant is referred to as bound-to-continuum design, or for short B-to-C design, and it provides a significantly wider gain spectrum than the bound-to-bound variant [34].

Furthermore, several different B-to-C active region designs can be stacked into a single QCL active region, thus providing an even further increased total width of the resulting overall gain spectrum [35, 36]. Figure 10 shows a compilation of lasing spectra recorded across the full tuning range of such a hetero-cascading QCL, comprising two B-to-C active region designs with different center wavelengths [37]. The spectra cover the 7.36-to-9.44-µm wavelength interval, corresponding to a relative tuning range of 25% around a center wavelength of 8.4 µm [37]. The corresponding tuning curve, i.e., output power-vs.-wavelength characteristic, is shown in Figure 11, together with the schematic gain spectra for the two different B-to-C sections. The double-humped tuning curve nicely reflects the two-stage hetero-cascading design of the QCL active region. An even wider tuning range extending from 7.6 µm to 11.4 µm, corresponding to a relative wavelength coverage of almost 40% has been achieved when using a hetero-cascading design, which combines five different B-to-C active region designs [38]. Exploiting the above highlighted freedom of design offered by the QCL technology, EC-QCLs are now becoming commercially available in different variants. They offer a wide tuning range in particular when operated in short-pulse or quasi-cw mode as well as cw operation mode, and mode-hop free tuning at the expense of a reduced tuning range [39].

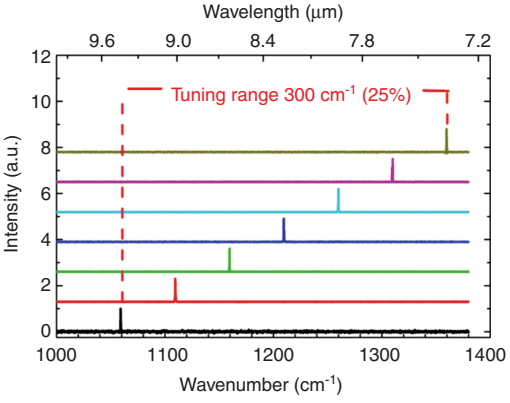

Figure 10 Lasing spectra of an EC-QCL comprising a hetero-cascading active region with two B-to-C stages, recorded across the full tuning range. The QCL chip was operated at room temperature in short pulse (100 ns pulse width) high repetition rate (1.1 MHz) quasi-cw mode [37].

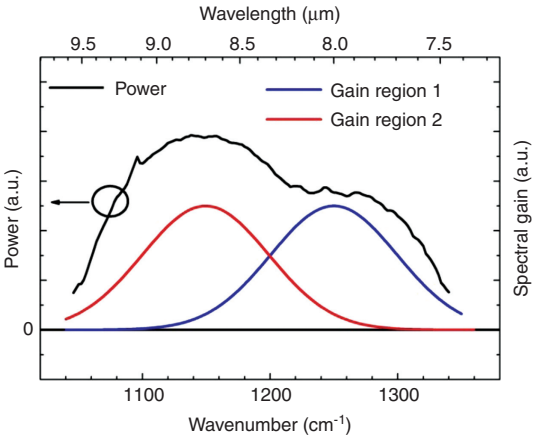

Figure 11 Output power-vs.-wavelength characteristic of an EC-QCL comprising a hetero-cascading active region with two B-to-C stages, together with the schematic gain spectra of the two B-to-C sections. The QCL was operated at room-temperature in short pulse (100 ns pulse width) high repetition rate (1.1 MHz) quasi-cw mode.

A current development objective is to reduce the form factor of external cavity semiconductor diode lasers, as well as to increase the wavelength tuning speed (or scan rate) by exploiting optical micro-electro-mechanical-system (MEMS) components for the wavelength-selective elements in the external cavity [40]. These components have been demonstrated mostly for devices operating in the wavelength bands around 1.5 µm, suitable for optical fiber-based telecommunication. Recently, there have been also realizations reported for wavelength-tunable semiconductor diode lasers emitting at wavelengths >2 µm [41]. In this implementation, an electrostatically actuated diffraction grating, micro-machined into silicon, has been employed as wavelength-selective element for wavelengths around 2.1 µm [41].

It appears to be straightforward to extend this approach to tunable lasers at longer wavelengths, in particular to EC-QCL. However, due to the scaling laws in optics, the fourfold increase in wavelength, from 2 µm to the earlier addressed MIR wavelength band around 8 µm, requires a corresponding increase in the size of the MEMS grating to maintain the same optical performance as well as spectral resolution. Such an increase in size of MEMS mirror or grating plates to a diameter in the 5-mm range is still challenging for current MEMS technology [42].

A first implementation of MEMS technology in EC-QCL has been reported in Ref. [43]. As illustrated in Figure 12, an electrostatically deflected plain MEMS mirror was used to direct the collimated output beam from the QCL chip onto a fixed diffraction grating. Wavelength tuning is achieved by tilting the MEMS mirror and thus varying the angle of incidence of the collimated beam on the grating. As the MEMS

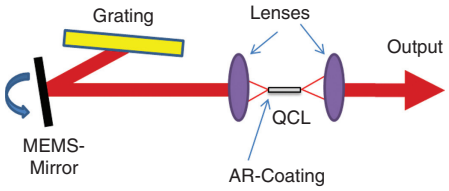

Figure 12 Schematic of an EC-QCL with a combination of tiltable MEMS mirror and fixed diffraction grating as tunable wavelength-selective feedback element [43].

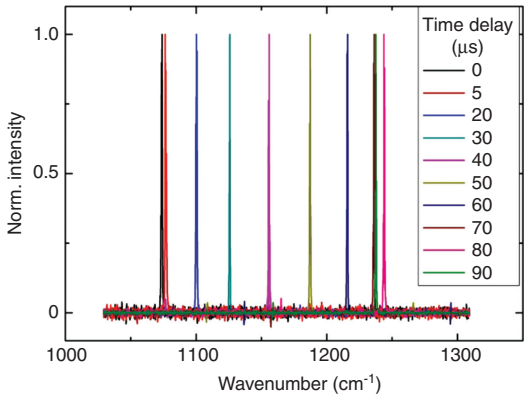

Figure 13 Lasing spectra recorded from the EC-QCL with MEMS mirror as schematically shown in Figure 12, taken at different delay times. Zero delay corresponds to that moment in time when the oscillating MEMS mirror is fully deflected [43].

mirror with a diameter of 3 mm is driven at its mechanical resonance frequency of 6 kHz (167 μs per cycle), very fast wavelength scans can be achieved. Figure 13 shows time-resolved lasing spectra recorded at different time delays, starting from the moment in time when the MEMS mirror is fully tilted. As can be seen from Figure 13, one full wavelength scan covering the 1070-to-1240-cm^{-1} frequency range can be achieved within 80 μs, which is half of the cycle time. Ongoing development in MEMS technology will allow replacement of the MEMS mirror used above by an appropriately designed scanning MEMS grating. This way, it will be possible to realize an optical MEMS based EC-QCL in the classical Littrow configuration.

5 EC-QCL-based active hyperspectral imaging for stand-off detection of explosives

In the following, we will introduce stand-off detection of residues of explosives as a prototype application of EC-QCLs in active hyperspectral imaging. Contactless sensing of hazardous substances, such as explosives, over a safe distance is still a challenging but tempting task. It has been shown that imaging MIR laser backscattering spectroscopy allows detection and identification of explosive residues on various kinds of surfaces [32, 37, 44–46]. Figure 14 shows the reflectance spectra of various explosives covering the 6.7-to-11-μm spectral range, recorded by conventional Fourier-transform IR (FTIR) reflectance spectroscopy, together with the transmission spectrum of air for that wavelength range [47]. It is obvious that these substances show distinct 'fingerprint spectra' within the 7.5-to-12-μm atmospheric transmission window and, hence, should allow detection and identification of explosives as well as distinguishing between explosives and harmless substances.

A schematic of the experimental setup used for imaging MIR laser backscattering spectroscopy is shown in Figure 15 [44]. A tunable EC-QCL is employed for the wavelength-selective illumination of the target area to be analyzed. Images of the target area with and without

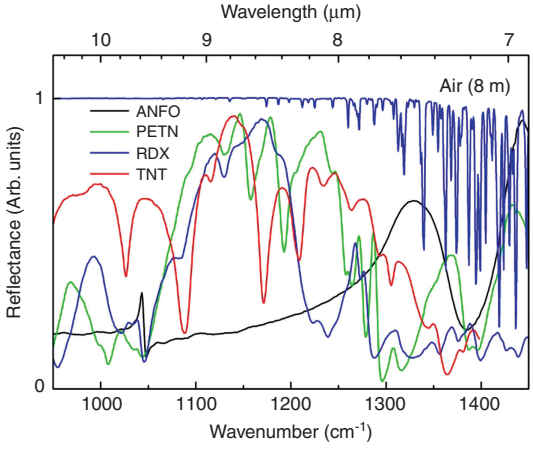

Figure 14 Reflectance spectra of four representative explosives covering the 6.7-to-11-μm wavelength range measured with FTIR spectroscopy. For wavelengths >7.5 μm, atmospheric transmission is sufficient for standoff detection over distances >10 m. ANFO denotes 'ammonium nitrate fuel oil', used mostly in improvised explosive devices, while PETN, RDX, and TNT are commercially available explosives [47].

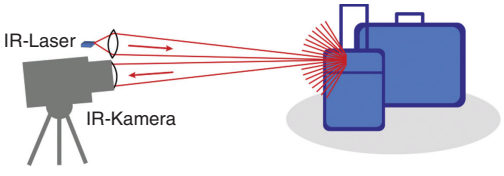

Figure 15 Schematic of an experimental setup used for imaging MIR laser backscattering spectroscopy [44].

illumination by the EC-QCL are recorded by a MIR camera for different illumination wavelengths. Subtracting consecutive images taken with and without laser illumination allows eliminating the signal stemming from thermal background radiation. Having recorded a complete set of the thus background-corrected MIR images covering the relevant wavelength range, the laser backscattering spectrum can be reconstructed for each pixel within the camera image. Figure 16 shows diffusive MIR laser backscattering spectra of the explosives RDX, TNT, and PETN [47]. Also shown in Figure 16 are selected lasing spectra, showing the wavelength tuning range of the EC-QCL used for wavelength selective illumination. Again, similar to the specular reflectance spectra shown in Figure 14, also the diffusive backscattering spectra allow a clear identification of the substances from which the laser light is backscattered. Using this technique, residues of explosives equivalent to a finger print can be detected and imaged over distances of several meters. The maximum detection range demonstrated so far using MIR laser backscattering spectroscopy is 20 m [43]. With this technique, the acquisition time for a full spectral set of images is typically a few seconds in the case of short-distance high-dose detection, while up to around 30 s for long-distance low-dose detection.

Exploiting the imaging capability of the MIR laser backscattering spectroscopy system shown in Figure 15, chemically sensitive and selective images of the surface of almost any object can be generated when using appropriate image analysis algorithms [48]. As an example, Figure 17 shows a chemically selective image extracted from the MIR backscattering data (cyan), overlaid with the passive MIR image of a computer mouse (dark blue).

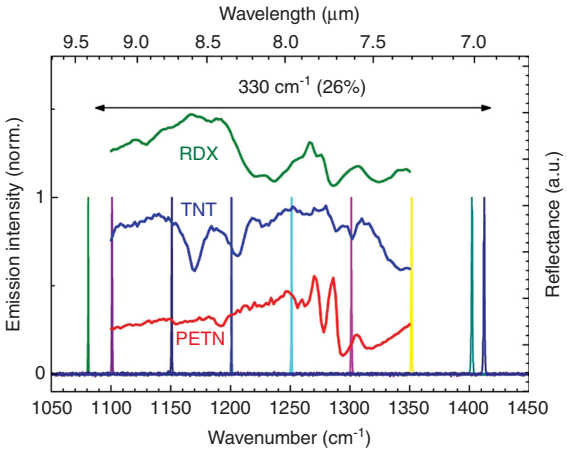

Figure 16 Diffusive MIR laser backscattering spectra of the explosives RDX, TNT, and PETN. Also shown is the tuning range of the EC-QCL used for wavelength-selective illumination, indicated by selected lasing spectra [47].

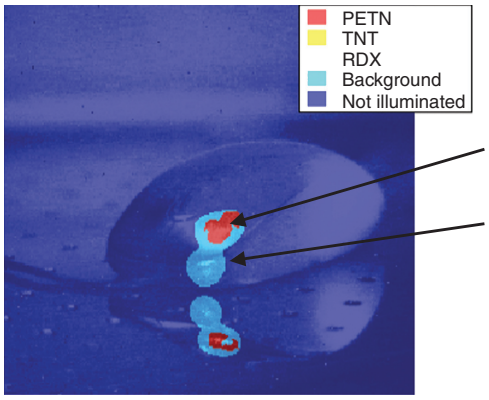

Figure 17 Imaging detection of a PETN fingerprint trace on the left button of a computer mouse using appropriate analysis algorithms. The target substance PETN was also detected in the reflection of the metal surface of the table the computer mouse is placed on [48].

In this example, the analysis algorithm was configured to detect the substances PETN, TNT, and RDX within the illuminated area of the scene. Positive detections on the mouse button were observed for PETN only. Locations where PETN was detected are marked in red. The other explosives did not present in the scene, and no corresponding false alarms were generated by the system. It is interesting to note that the contaminated area was also detected in the mirror reflection by the metal surface of the table on which the analyzed object was placed [48].

6 Conclusions

Since their first experimental realization in 1994, quantum cascade lasers (QCLs) have matured into a ready-to-use laser technology, covering in particular the mid-infrared (3.5–12 µm) wavelength range. Being an electrically injected semiconductor laser variant and benefiting from the economy of scale associated with wafer level semiconductor batch process technologies, very compact laser modules and systems can be realized. As QCLs are based on intersubband transitions within the conduction band of quantum mechanically engineered semiconductor nano-structures, the aforementioned wide wavelength span can be covered based on a single semiconductor material system (GaInAs/AlInAs/InP materials combination). Furthermore, the width of the gain spectrum can be engineered, allowing the realization of broadband tunable EC-QCLs, which are ideally suitable for molecular spectroscopy of not only gases but also liquids and solids.

Concerning active imaging, QCLs can be used as a multiple-Watt illumination source. They can be operated

in both cw and short pulse mode with a spectral width of typically 1%–2% of the lasing wavelength. Alternatively, QCLs can be operated as tunable, spectrally highly selective laser sources when using the EC-QCL variant. This way, QCLs can be used as a wavelength-agile illumination source, enabling active hyperspectral imaging. A representative example for spectroscopic active imaging is the use of MIR laser backscattering spectroscopy for the stand-off detection of hazardous substances, such as explosives.

Acknowledgments: The authors would like to thank R. Aidam, W. Bronner, R. Driad, S. Hugger, J. Jarvis, C. Schilling, and R. Ostendorf for valuable contributions as well as the German Ministry for Education and Research (BMBF) and the European Commission for continued project funding.

Received January 13, 2014; accepted February 24, 2014; previously published online March 14, 2014

References

[1] For a recent review see, e.g. Jerome Faist, 'Quantum Cascade Lasers', (Oxford University Press, Oxford, 2013).
[2] F. Capasso, SPIE Opt. Eng. 49, 111102 (2010).
[3] M. Razeghi, Y. Bai, S. Slivken and S.R. Darvish, SPIE Opt. Eng. 49, 111103 (2010).
[4] A. Lyakh, R. Maulini, A. G. Tsekoun and C. K. N. Patel, SPIE Opt. Eng. 49, 111105 (2010).
[5] Y. Bai, N. Bandyopadhyay, S. Tsao, S. Slivken and M. Razeghi, Appl. Phys. Lett. 98, 181102 (2011).
[6] M. Troccoli, X. Wang and J. Fan, SPIE Opt. Eng. 49, 111106 (2010).
[7] R. P. Leavitt, J. L. Bradshaw, K. M. Lascola, G. P. Meissner, F. Micalizzi, et al., SPIE Opt. Eng. 49, 111109 (2010).
[8] A. Lyakh, R. Maulini, A. Tsekoun, R. Go, C. Kumar, et al., Opt. Exp. 20, 24272–24279 (2012).
[9] F. Xie, C. Caneau, H. P. Leblanc, D. P. Caffey, L. C. Hughes, et al., IEEE J. Sel. Topics Quantum Electron. 19, 120407 (2013).
[10] see e.g. G. P. Agrawal and N. K. Dutta, 'Semiconductor Lasers', Chapter 7 and references therein, (Van Nostrand Reinhold, New York, 1993).
[11] J. Faist, C. Gmachl, F. Capasso, C. Sirtori, D. L. Sivco, et al., Appl. Phys. Lett. 70, 2670–2672 (1997).
[12] C. Gmachl, F. Capasso, J. Faist, A. L. Hutchinson, A. Tredicucci, et al., Appl. Phys. Lett. 72, 1430–1432 (1998).
[13] Ch. Mann, Q. K. Yang, F. Fuchs, W. Bronner, R. Kiefer, et al., Proc. SPIE 5365, 173–182 (2004)
[14] Ch. Mann, Q. Yang, F. Fuchs, W. Bronner, K. Köhler and J. Wagner, tm – Technisches Messen 72, 356–365 (2005).
[15] Q. K. Yang, W. Bronner, C. Manz, B. Raynor, H. Menner, et al., Appl. Phys. Lett. 88, 201109 (2006).
[16] See, e.g. T. Beyer, M. Braun and A. Lambrecht, J. Appl. Phys. 93, 3158–3160 (2003).
[17] S. Blaser, D. A. Yarekha, L. Hvozdara, Y. Bonetti, A. Muller, et al., Appl. Phys. Lett. 86, 041109 (2005); for commercial availability of DFB-QCL, see e.g.: http://www.alpeslasers.ch/; http://www.atoptics.com
[18] A. Wittmann, M. Giovannini, J. Faist, L. Hvozdara, S. Blaser, et al., Appl. Phys. Lett. 89, 141116 (2006).
[19] B. G. Lee, M. A. Belkin, C. Plügl, L. Diehl, H. A. Zhang, et al., IEEE J. Quantum Elect. 45, 554–565 (2009).
[20] P. Rauter, S. Menzel, B. Gokden, A. K. Goyal, C. A. Wang, et al., Appl. Phys. Lett. 102, 181102 (2013).
[21] P. Rauter, S. Menzel, A. Goyal, B. Gokden, C. A. Wang, et al., Appl. Phys. Lett. 101, 261117 (2012).
[22] B. G. Lee, J. Kansky, A. K. Goyal, C. Pflügl, L. Diehl, et al., Opt. Exp. 17, 16216–16224 (2009).
[23] A. K. Goyal, M. Spencer, O. Shatrovoy, B. G. Lee, L. Diehl, et al., Opt. Exp. 19, 26725–26732 (2011).
[24] A. Lyakh, R. Maulini, A. Tsekoun, R. Go and C. K. N. Patel, Opt. Exp. 22, 1203–1208 (2014).
[25] T. Mansuripur, S. Menzel, R. Blanchard, L. Diehl, C. Pflugl, et al., Opt. Exp. 20, 23339–23348 (2012).
[26] S. Slivken, N. Bandyopadhyay, S. Tsao, S. Nida, Y. Bai, et al., Appl. Phys. Lett. 100, 261112 (2012).
[27] M. C. Zheng, P. Q. Liu, X. Wang, J.-Y. Fan, M. Troccoli, et al., Appl. Phys. Lett. 103, 211112 (2013).
[28] see e.g. Cunyun Ye, 'Tunable External Cavity Diode Lasers', (World Scientific Pub. Co., New Jersey, 2004).
[29] G. P. Luo, C. Peng, H. Q. Le, S. S. Pei, W.-Y. Hwang, et al., Appl. Phys. Lett. 78, 2834–2836 (2001).
[30] R. Maulini, M. Beck, J. Faist and E. Gini, Appl. Phys. Lett. 84, 1659–1661 (2004).
[31] M. G. Littman and H. J. Metcalf, Appl. Opt. 17, 2224–2227 (1978).
[32] B. Hinkov, F. Fuchs, Q. K. Yang, J. Kaster, W. Bronner, et al., Appl. Phys. B 100, 253–260 (2010).
[33] G. Wysocki, R. F. Curl, F. K. Tittel, R. Maulini, J. M. Bulliard, et al., Appl. Phys. B 81, 769–777 (2005).
[34] J. Faist, M. Beck, T. Aellen, and E. Gini, Appl. Phys. Lett. 78, 147–149 (2001).
[35] C. Gmachl, D. Sivco, J. Baillargeon, A. Hutchinson, F. Capasso, et al., Appl. Phys. Lett. 79, 572–574 (2001).
[36] A. Wittmann, A. Hugi, E. Gini, N. Hoyler, and J. Faist, IEEE J. Quantum Electron. 44, 1083–1088 (2008).
[37] F. Fuchs, S. Hugger, M. Kinzer, Q. K. Yang, W. Bronner, et al., Proc. SPIE 82681, 82681N-1 (2012).
[38] A. Hugi, R. Terazzi, Y. Bonetti, A. Wittmann, M. Fischer, et al. Gini; Appl. Phys. Lett. 95, 061103 (2009).
[39] T. Day, M. Weida, D. Arnone and M. Pushkarsky, Proc. SPIE 7319, 73190F (2009).
[40] A. Q. Liu and X. M. Zhang, J. Micromech. Micro Eng. 17, R1 (2007).
[41] E. Geerlings, M. Rattunde, J. Schmitz, G. Kaufel, J. Wagner, et al., IEEE J. Quantum Electron. 44, 1071–1075 (2008).
[42] J. Grahmann, H. Schenk, A. Merten, M. Fontenot, R. Ostendorf, et al., Proc. SPIE 8977-6, (2014).
[43] S. Hugger, F. Fuchs, J. Jarvis, M. Kinzer, Q. K. Yang, et al., Proc. SPIE 8631, 86312I (2013).

[44] F. Fuchs, S. Hugger, M. Kinzer, R. Aidam, W. Bronner, et al., SPIE Opt. Eng. 49, 111127 (2010).
[45] C. W. Van Neste, L. R. Senesac and T. Thundat, Appl. Phys. Lett. 92, 234102 (2008).
[46] R. Furstenberg, C. Kendziora, J. Stepnowski, S. Stepnowski, M. Rake, et al., Appl. Phys. Lett. 93, 224103 (2008).
[47] F. Fuchs, S. Hugger, Q. K. Yang, J.-P. Jarvis, M. Kinzer, et al., in 'The Wonder of Nanotechnology: Present and Future of Optoelectronics Quantum Devices and their Applications for Environment, Health, Security, and Energy', Ed. by M. Razeghi, L. Esaki and K. von Klitzing (SPIE Press Book Volume: PM238, ISBN: 9780819495969, Bellingham, WA, 2013) p. 645.
[48] J. Jarvis, F. Fuchs, S. Hugger, V. Blattmann, Q. K. Yang, et al., in 'Proceedings of the 8th Security Research Conference Future Security', (Fraunhofer Verlag, 2013) p. 205.

Quankui Yang received his PhD degree in Solid-State Electronics from the Chinese Academy of Sciences, Shanghai, China, in 2000. After that, he joined the Fraunhofer Institute for Applied Solid-State Physics (IAF), Freiburg, Germany, as a research scientist. His work mainly focuses on the development and application of infrared semiconductor lasers in particular quantum cascade lasers. His interests also include other semiconductor devices such as infrared detectors, heterojunction bipolar transistors, and backward diodes. Dr. Yang is a co-inventor of three patents, has co-authored more than 70 peer-reviewed journal papers, and contributed to an edition of Landolt-Börnstein dedicated to quantum cascade lasers.

Frank Fuchs received his PhD degree in Physics from Freiburg University, Freiburg, Germany, in 1991. Since then, he has carried out applied research at the Fraunhofer Institute for Applied Physics (IAF), Freiburg, Germany. During 2004–2005, he worked as a Visiting Scientist at the Center for Quantum Devices at Northwestern University, Evanston, IL, USA. His research interests include work on infrared devices based on low gap semiconductors. More recently, he has been concentrating on standoff detection of hazardous substances using broadband tunable quantum cascade lasers. He has co-authored more than 100 refereed journal articles and two book chapters, he has contributed to an edition of Landoldt-Börnstein, and presented 17 invited talks on international conferences.

Joachim Wagner received the PhD degree in Physics from the University of Stuttgart, Stuttgart, Germany, in 1982. From 1982 to 1984 he worked at the "Max-Planck-Institut für Festkörperforschung", Stuttgart, Germany, in the group of Prof. M. Cardona before joining the Fraunhofer-Institut for Applied Solid State Physics, Freiburg, Germany, in 1985. There he is currently deputy director and head of the Department of "Optoelectronic Modules". He is also Professor at the Institute of Physics of the University of Freiburg and an associated member of the Materials Research Center Freiburg (FMF). His current research interests include III/V-semiconductor heterostructures and their application in optoelectronic devices both for the infrared and the visible/uv spectral range. He is author or coauthor of more than 450 scientific publications including several review papers and book chapters.